Acta Biomed 2021; Vol. 92, Supplement 4: e2021411 DOI: 10.23750/abm.v92iS4.12115

Original article

The Modular Concept in Skull Base Surgery: Anatomical Basis of the Median, Paramedian and Lateral Corridors

Alice Giotta Lucifero[1], Juan C Fernandez-Miranda[2], Maximiliano Nunez[2], Nunzio Bruno[3], Nicola Tartaglia[4], Antonio Ambrosi[4], Gian Luigi Marseglia[5,6], Renato Galzio[7], Sabino Luzzi[1,8]

[1] Neurosurgery Unit, Department of Clinical-Surgical, Diagnostic and Pediatric Sciences, University of Pavia, Pavia, Italy; [2] Department of Neurological Surgery, Stanford University, Stanford, California, USA; [3] Division of Neurosurgery, Azienda Ospedaliero Universitaria Consorziale Policlinico di Bari, Bari, Italy; [4] Surgical Unit, Department of Medical Sciences, University of Foggia, Foggia, Italy; [5] Pediatric Clinic, Department of Pediatrics, Fondazione IRCCS Policlinico San Matteo, University of Pavia, Pavia, Italy; [6] Department of Clinical, Surgical, Diagnostic and Pediatric Sciences, University of Pavia, Pavia, Italy; [7] Neurosurgery Unit, Maria Cecilia Hospital, Cotignola, Italy; [8] Neurosurgery Unit, Department of Surgical Sciences, Fondazione IRCCS Policlinico San Matteo, Pavia, Italy.

Abstract. *Introduction*: A thorough understanding of skull base anatomy is imperative to perform safely and effectively any skull base approach. In this article, we examine the microsurgical anatomy of the skull base by proposing a modular topographic organization in the median, paramedian, and lateral surgical corridors in relation to transcranial and endoscopic approaches. *Methods*: Five dry skulls were studied focusing on the intracranial and exocranial skull base. Two lines were drawn parallel to the lateral border of the cribriform plate of the ethmoid bone and foramen lacerum, respectively. Lines 1 and 2 delimited the median, paramedian and lateral corridors of the skull base. The bony structures that formed each corridor were carefully reviewed in relation to the planning and execution of the skull base transcranial and endoscopic approaches. *Results*: The midline corridor involves the crista galli, cribriform plate, planum and jugum sphenoidale, chiasmatic sulcus, tuberculum sellae, sellar region, dorsum sellae, clivus, and foramen magnum. The paramedian corridor includes the fovea ethmoidalis, the root of the lesser and greater sphenoid wing, anterior clinoid process, foramen lacerum, the upper half of the petro-occipital suture, and jugular tubercle. The lateral corridors include the orbital plates, sphenoid wings, squamosal and petrous parts of the temporal bone, caudal aspect of the petro-occipital suture, internal auditory canal, jugular foramen, the sulcus of the sigmoid sinus. *Conclusion:* In-depth three-dimensional knowledge of skull base anatomy based on the modular concept of the surgical corridors is critical for the planning and execution of the transcranial and endoscopic approaches.

Key words: Anterior Skull Base; Endoscopic Skull base Approaches, Foramen Magnum, Jugular Foramen, Jugular Tubercle, Middle Skull Base, Posterior Skull Base.

Introduction

The skull is composed of the splanchnocranium, or the facial skeleton, and the neurocranium, which surrounds the cerebral structures. The neurocranium is divided further into the calvaria and the cranial base by a plane passing through the glabella to the external occipital protuberance.

The calvaria is formed by the frontal, parietal, temporal, and occipital bones and part of the greater sphenoid wings. The cranial base is composed of the frontal, ethmoid, temporal, and occipital bones, all of which join with the sphenoid bone in the center of the skull base. The cranial base has an exocranial and endocranial surface, which are connected by channels and foramina traversed by nerves, arteries, and veins.

The endocranial surface is classically divided into the anterior, middle, and posterior fossae. The exocranial surface borders the orbit, nasal cavity, nasopharynx, and infratemporal, pterygopalatine, and mandibular fossae (1-14).

An overview of the anatomy of the skull base and modular topographic organization in the median, paramedian, and lateral surgical corridors as they relate to transcranial end endoscopic approaches are herein reported.

Methods

Five dry skulls of unknown age and gender were used for the study. The calvaria was removed to examine the endocranial surface of the anterior, middle, and posterior fossa. The corresponding exocranial surface of each fossa was also studied in detail.

On the endocranial surface, a line was traced at the level of the lateral border of the horizontal plate of the ethmoid bone and continued down to the foramen magnum. This line was called line 1. At the exocranial side, line 1 was drawn at the roof of the nasal cavity at the lateral limit of the cribriform plate of the ethmoid and extended inferiorly to meet the ipsilateral sphenopetrosal suture. On the endocranial surface, line 2 was traced parallel to the lateral edge of the foramen lacerum and directed toward the anterior and posterior fossa. On the exocranial side, line 2 intercepts the lateral border of the lateral pterygoid plate of the sphenoid bone. The area in between the two lines 1 is the median skull base corridor, whereas the area ranging from line 1 and line 2 forms the paramedian corridor. The region of the skull base lateral to line 2 corresponds to the lateral corridor. The bony structures forming each corridor were carefully reviewed in relation to the planning and execution of the transcranial and endoscopic skull base approaches.

Results

Overview of the Anterior, Middle, and Posterior Skull Base

The anterior skull base is composed of the frontal, ethmoid, and sphenoid bones which articulate at the frontoethmoidal, sphenoethmoidal, and sphenofrontal sutures. The frontal bone forms the roof of the orbit and is immediately beneath the rectus gyri and orbital cortex. The ethmoid bone articulates in the midline with the frontal bone. The posterior portion of the endocranial surface of the anterior skull base is completed posteriorly by the lesser sphenoid wings, anterior clinoid processes, and the planum and jugum sphenoidale.

The middle skull base is composed of the sphenoid and temporal bones, which articulate at the sphenopetrosal and sphenosquamosal sutures.

The posterior skull base is formed by the sphenoid, temporal, and occipital bones, which articulate at the spheno-occipital, temporomastoid, occipitomastoid, and petro-occipital (petroclival) sutures.

On the endocranial surface, the anterior and middle skull base are separated by the sphenoid ridges laterally, the anterior clinoid processes in the paramedian region, and the jugum sphenoidale in the midline. The border between the middle and posterior skull base is given by a line traced along the posterior-superior edge of the petrous part of the temporal bone laterally, and the posterior clinoid processes and dorsum sellae.

The conventional division between the anterior and middle skull base on the exocranial surface corresponds to a line drawn at the level of the pterygomaxillary fissures going down to the posterior edges of the alveolar processes of the maxillae; in the paramedian corridor, the line follows the inferior border of the choanae to end at the level of the posterior nasal spine. The border between the middle and posterior skull base is traced by a line drawn oblique medially and forward passing through the mastoid tip, stylomastoid foramen, external orifice of the carotid canal, and foramen lacerum. In the midline, the border is delineated by a line passing along the posterior border of the vomer–sphenoid junction **(Figure 1)**.

Median Skull Base Corridor

From the transcranial perspective, the median anterior skull base corridor is formed by the frontal crest of the frontal bone, crista galli, and cribriform plate of the ethmoid bone, and planum and jugum sphenoidale. The crista galli serves as a point of attachment for the falx cerebri and the superior and inferior

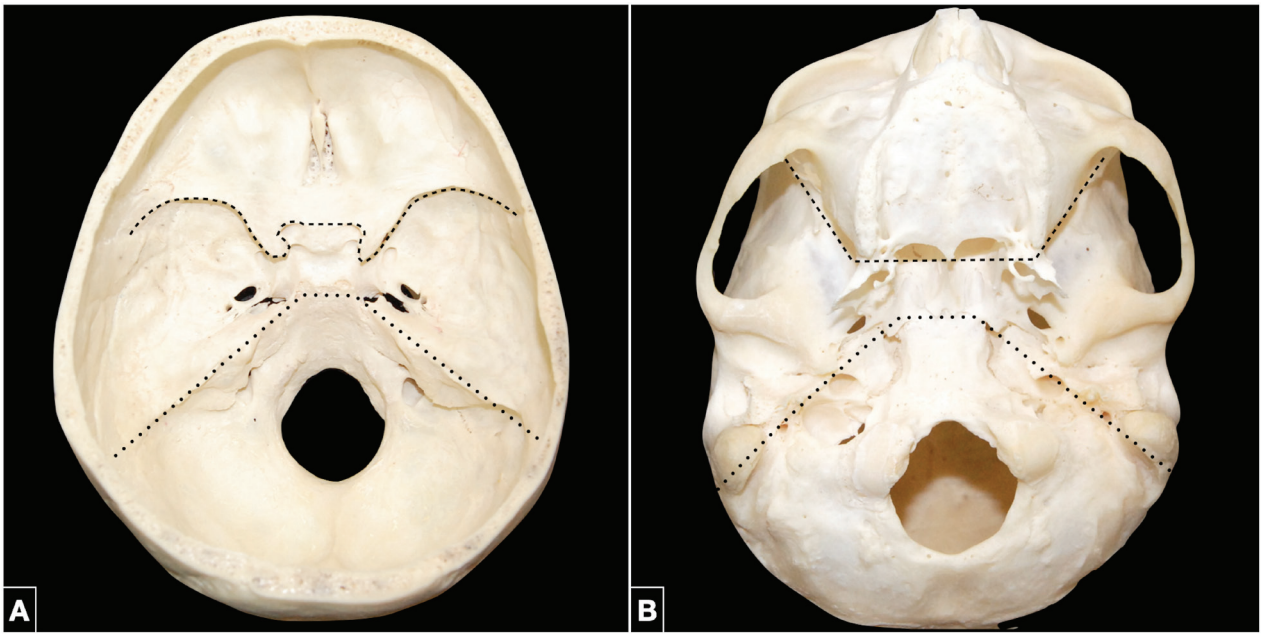

Figure 1. (A) Endocranial surface of the skull base. The border between the anterior and middle skull base is marked, from lateral to medial, by the sphenoid ridges, the anterior clinoid processes, and the jugum sphenoidale in the midline (dotted line). The middle and posterior skull base are separated by a line along the posterosuperior edge of the petrous ridges laterally and the posterior clinoid processes and dorsum sellae in the medially (pointed line). (B) Exocranial surface of the skull base. The anterior and middle skull base are separated by a transverse line extending through the pterygomaxillary fissures and the posterior edges of the alveolar processes of the maxillae laterally, the inferior border of the choanae in the paramedian corridor, and the posterior nasal spine in the midline (dotted line). The border between the middle and posterior skull base is marked by the mastoid tip, stylomastoid foramen, external orifice of the carotid canal, foramen lacerum, and the vomer–sphenoid junction in the midline (pointed line).

sagittal sinuses. The cribriform plate transmits the olfactory fila. Between the crista galli and the cribriform plate, the foramen cecum may rarely transmit the persistent anterior nasal emissary vein, when present. The planum and jugum sphenoidale form the roof of the sphenoid sinus (Figure 2A).

The median middle skull base corridor is formed, from anterior to posterior, by the chiasmatic sulcus on the superior aspect of the body of the sphenoid bone, tuberculum sellae, sella, and dorsum sellae. At the lateral ends of the chiasmatic sulcus, the optic canals transmit the optic nerves and the ophthalmic arteries from the intracranial space to the orbits. The anterior and posterior limbs of the chiasmatic sulcus are also referred to as the jugum sphenoidale and tuberculum sellae, respectively. The sellar region consists of a deep rounded depression in the sphenoid body containing the pituitary gland. The sella is delineated posteriorly by the dorsum sellae, the lateral and uppermost parts of which are known as the posterior clinoid processes (Figure 3A).

The median posterior skull base corridor involves the clivus and the foramen magnum. The anatomical boundaries of the clivus are the dorsum sellae of the sphenoid bone superiorly, the petroclival sutures laterally, and the anterior border of the foramen magnum inferiorly. The most caudal point of the clivus, which corresponds to the most anterior part of the foramen magnum in the midline, is referred to as the basion. The basilar part of the occipital bone forms the lower two-thirds of the clivus; the posterior surface of the sphenoid body (dorsum sellae) forms the upper third. The basilar part of the occipital bone and the sphenoid body articulate at the spheno-occipital synchondrosis. In adults, the division between the two bones is not appreciable because physiological closure of the spheno-occipital synchondrosis is well underway by the age of 15 years, and complete by 17 years (15). On a sagittal view, the basilar (or clival) part of the occipital bone is oriented anteriorly and superiorly at a 45° angle. When viewed from behind, the clivus is concave

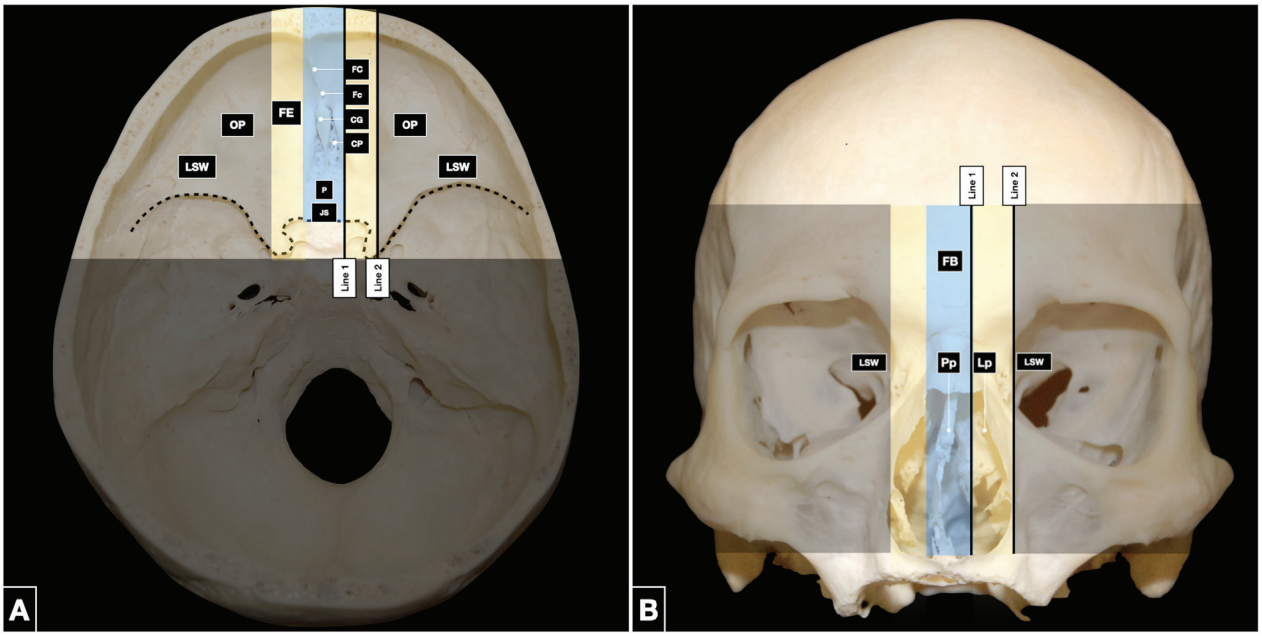

Figure 2. (A) The endocranial surface of the anterior skull base is divided into medial, paramedian, and lateral corridors. The central corridor (light blue) is composed of the frontal crest of the frontal bone, crista galli and cribriform plate of the ethmoid bone, and planum and jugum sphenoidale. The paramedian corridor (yellow) involves the fovea ethmoidalis. The lateral corridor (black) is composed of the orbital plates of the frontal bone anteriorly and the lesser sphenoid wings laterally. The boundary between the anterior and middle skull base is delineated by the dotted line. (B) The exocranial surface of the anterior skull base is composed in the midline (light blue) by the frontal, ethmoid and sphenoid bones. The perpendicular plate of the ethmoid bone joined to the vomer, forms the upper part of the nasal septum. The lateral plates of the ethmoid bone are in the paramedian region (yellow) and divide the nasal cavity from the orbits. The lateral corridor (black) is composed of the orbital plates of the frontal bone and the lesser sphenoid wings. CG: crista galli, CP: cribriform plate, EB: ethmoid bone, FB: frontal bone, FC: frontal crest, Fc: Foramen cecum, FE: fovea ethmoidalis, JS: jugum sphenoidale, Lp: lateral plates, LSW: lesser sphenoid wings, OP: orbital plates, P: planum, Pp: perpendicular plate, SB: sphenoid bone

from side to side; the central concavity is known as the *central clival depression*. This region is very difficult to reach surgically at the midclivus level (16, 17). The conventional border between the upper and middle clivus coincides with a horizontal line traced at the level of the petrous apex; a line passing through the glossopharyngeal notch of the jugular foramen delineates the middle and lower clivus (18). Intradurally, the same limits are given by the exit point of the abducens nerve through the dura, located 3.4 millimeters below the posterior-superior border of the petrous part of the temporal bone, and the entry point of the glossopharyngeal nerve in the jugular foramen, respectively (18).

The foramen magnum is bounded by the basilar, lateral, and squamosal parts of the occipital bone. The anterior border is formed by the inferior third of the clivus; the lateral limits are formed by the jugular tubercles, which are thought to be the result of the fusion between the basilar and lateral (condylar) parts of the occipital bone. The posterior border is formed by the most caudal aspect of the squamosal part of the occipital bone. The opisthion is the most posterior point of the foramen magnum in the midline. The structures passing through the foramen magnum are the upper cervical spinal cord, spinal accessory nerves, vertebral arteries, and anterior and posterior spinal arteries (Figure 4A).

From the endoscopic endonasal perspective, the median anterior skull base is composed mainly of the frontal, ethmoid, and sphenoid bones. The frontal and the ethmoid bones constitute the anterior two-thirds of the roof of the nasal cavity; the sphenoethmoidal recess comprises the posterior third (Figure 2B).

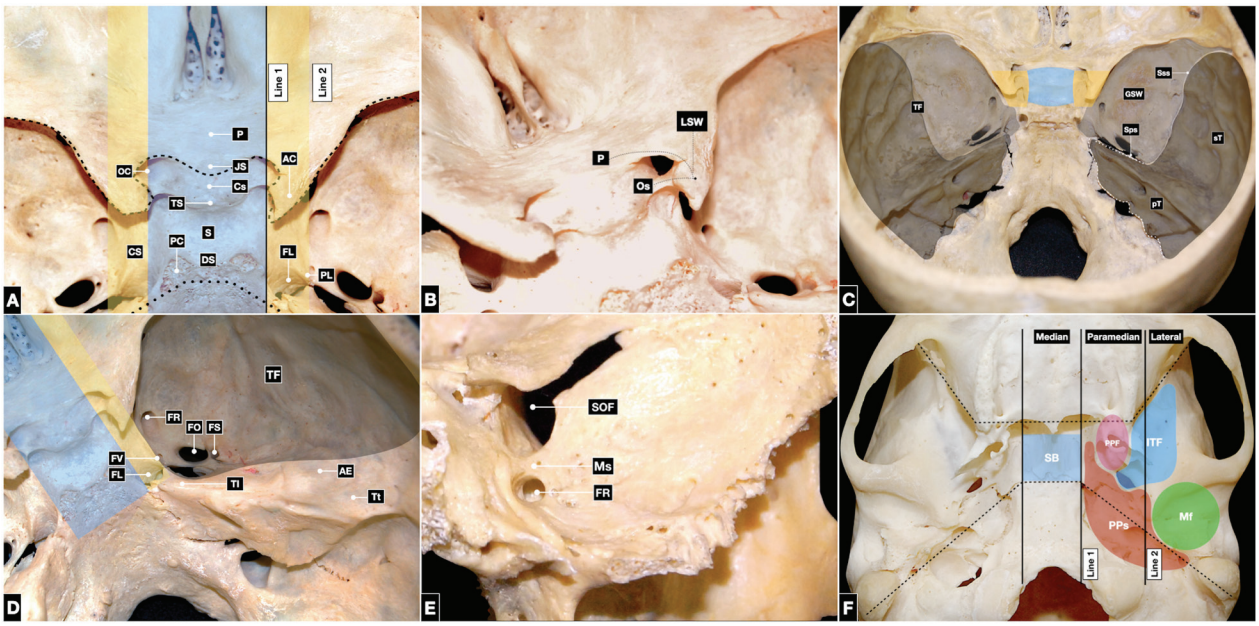

Figure 3. Endocranial surface of the middle skull base. (A) The median corridor (light blue) involves, from anterior to posterior, the chiasmatic sulcus, tuberculum sellae, sellar region, and dorsum sellae; the posterior clinoid processes comprise the superolateral parts of the dorsum sellae. The openings of the optic canals are located at the lateral ends of the chiasmatic sulcus. The paramedian region (yellow) is composed of the root of the lesser and greater sphenoid wings and the anterior clinoid processes anteriorly, and the foramen lacerum posteriorly. This region contains the carotid sulcus, which contains the cavernous segment of the internal carotid artery above the petrolingual ligament. The petrolingual ligament marks the border between the lacerum and cavernous segments of the internal carotid artery and attaches to the lingula of the sphenoid bone. Boundaries between anterior and middle (dotted line), and middle and posterior skull base (pointed line). (B) The lateral region (black) is composed of the lesser and greater sphenoid wings and the superior orbital fissure in between. In the lateral corridor, the squamous and petrous parts of the temporal bone form the temporal fossa, which contains the foramen rotundum, foramen ovale, foramen spinosum, and occasionally the foramen of Vesalius, when present. The most lateral portion is composed of the superior surface of the petrous part of the temporal bone. At the petrous apex, the trigeminal impression houses Meckel's cave, which contains the Gasserian ganglion. Laterally, the arcuate eminence overlies the superior semicircular canal; the tegmen tympani separates the middle skull base from the middle ear. (C) The optic strut is the root of the lesser sphenoid wing and is located on the lateral surface of the body of the sphenoid bone; it separates the optic canal from the superior orbital fissure. (D) The maxillary strut separates the foramen rotundum from the superior orbital fissure. (E) The median or sellar (light blue), paramedian or parasellar (yellow), and lateral (black) corridors of the middle skull base. The lateral region is formed by the sphenoid bone and squamous and petrous part of the temporal bone, which articulate at the sphenopetrosal and sphenosquamosal sutures. (F) The exocranial surface of the middle skull base. The median corridor (light blue) involves the inferior side of the body of the sphenoid bone. The paramedian corridor (yellow) is composed of the pterygoid process of the sphenoid bone, which branches into medial and lateral pterygoid plates; the pterygoid fossa is located between the plates. The lateral corridor (black) is comprised of the infratemporal fossa anteriorly and the mandibular fossa posteriorly. The exocranial surface of the middle skull base also borders the parapharyngeal space. The boundaries between the anterior and middle skull base and the middle and posterior skull base are delineated by dotted and pointed lines, respectively. AC: anterior clinoid, AE: arcuate eminence, CS: carotid sulcus, Cs: chiasmatic sulcus, DS: dorsum sellae, FL: foramen lacerum, FO: foramen ovale, FR: foramen rotundum, FS: foramen spinosum, FV: foramen of Vesalius, GSW: greater sphenoid wing, ITF: infratemporal fossa, JS: jugum sphenoidale, LWS: less sphenoid wing, MF: mandibular fossa, OC: optic canal, Os: optic strut, P: planum, PC: posterior clinoid, Pf: pterygoid fossa, PL: petrolingual ligament, PP: pterygoid process, PPS: parapharyngeal space, pT: petrous part of the temporal bone, S: sella, SB: sphenoid body, SOF: superior orbital fissure, Sps: sphenopetrosal suture, Sss: sphenosquamosal suture, sT: squamous and petrous part of the temporal bone, TF: temporal fossa, TI: trigeminal impression, TS: tuberculum sellae, Tt tegmen tympani.

The median middle skull base is mainly composed of the inferior aspect of the body of the sphenoid bone, sphenoid sinus, and sellar floor. The exocranial middle skull base borders with the pterygopalatine, infratemporal, and mandibular fossae and the parapharyngeal space (Figure 3F). At the level of the median posterior

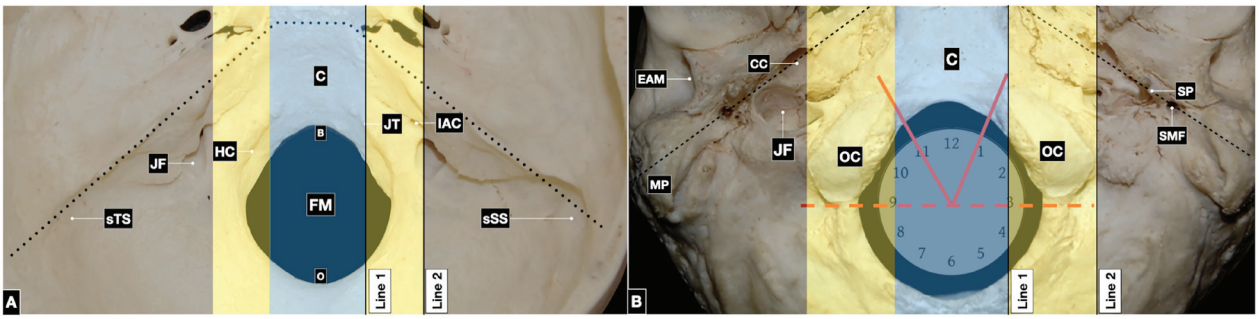

Figure 4. (A) Endocranial surface of the posterior skull base. The central corridor (light blue) includes the clivus and the foramen magnum. In the midline, the most anterior point of the foramen magnum on the clival part of the occipital bone is the basion; the most posterior point is the opisthion, located at the most caudal aspect of the squamosal part of the occipital bone. In the paramedian region (yellow) lie the jugular tubercle and the hypoglossal canal. The lateral corridor (black) contains the jugular foramen, bordered by the notch of the jugular process of the occipital bone and the jugular fossa of the petrous part of the temporal bone. On the posterior surface of the petrous bone, the internal auditory canal is located above the jugular foramen. The sulcus of the transverse and sigmoid sinuses courses lateral to medial toward the jugular foramen along the surface of the squamous part of the temporal bone. The boundary between the middle and posterior skull base is delineated by a pointed line. (B) The exocranial surface of the posterior skull base. The midline corridor (light blue) is occupied by the clivus and foramen magnum. The paramedian corridor (yellow) involves the occipital condyles. The condyles are oval-shaped, articulate with the superior articular facet of the atlas, and oriented anteriorly and medially from three to one and nine to eleven o'clock. The exocranial posterolateral skull base (black) is formed by the styloid, mastoid, and petrous parts of the temporal bone, and the squamosal part of the occipital bone. Anteromedially, it contains the external orifice of the carotid canal; posterior to this lie the jugular foramen and hypoglossal canal, which open into the parapharyngeal space. Posterior to the styloid process is the opening of the stylomastoid foramen. The mastoid process constitutes the posterior border of the external acoustic meatus. The boundary between the middle and posterior skull base is delineated by a pointed line. B: basion, C: clivus, CC: carotid canal, EAM: external acoustic meatus, FM: foramen magnum, HC: hypoglossal canal, IAC: internal auditory canal, JF: jugular foramen, JT: jugular tuberculum, MP: mastoid process, O: opisthion, OC: occipital condyle, SMF: stylomastoid foramen, SP: styloid process, sSS sulcus of the sigmoid sinus, sTS: sulcus of the transverse sinus.

skull base, the outer surface of the clivus is convex-shaped. Its transnasal frontal view is widely limited by the pterygoid processes of the sphenoid bone. The lower clivus is wider than the upper and mainly consists of the exocranial surface of the basioccipital bone. In the midline, at an average distance of 1 cm from the basion, the superior constrictor muscle of the pharynx attaches to the pharyngeal tubercle (Figure 4B).

Paramedian Skull Base Corridor

At the endocranial side, the paramedian anterior skull base corridor is formed by the fovea ethmoidalis of the frontal bone, which is the roof of the ethmoid air cells. Here, the anterior and posterior ethmoidal foramina give passage to the anterior and posterior ethmoidal arteries and nerves, respectively. The perpendicular plate attaches to the vomer and contributes to the formation of the upper portion of the nasal septum, which divides the nasal cavity in the midline **(Figure 2)**.

Anteriorly, the paramedian middle skull base corridor involves the lateral aspect of the body of the sphenoid bone, which is the root of the lesser and greater sphenoid wings; posteriorly, it is comprised of the foramen lacerum. The carotid sulcus of the sphenoid bone is also within the paramedian corridor and extends from the petrolingual ligament forward to the paraclinoid region. The foramen lacerum is formed by the union between the petrous apex, the uppermost part of the petroclival fissure, and the lateral aspects of the dorsum sellae. The greater superficial petrosal nerve joins the deep petrosal nerve from the sympathetic plexus around the petrous internal carotid artery to form the vidian nerve at the level of the foramen lacerum. Meningeal branches from the ascending pharyngeal artery pass through the foramen lacerum, along with emissary veins connecting the cavernous sinus, inferior petrosal sinus, and basilar plexus to the

pterygoid plexus. In the parasellar region, the roof of the cavernous sinus is formed by the anterior clinoid process anteriorly and the oculomotor triangle posteriorly. The lingula of the sphenoid bone provides a site of attachment for the petrolingual ligament, which marks the border between the lacerum and cavernous segments of the internal carotid artery (Figure 3A, B, D). The paramedian posterior skull base corridor involves the superior half of the petro-occipital suture and the jugular tubercle. Inferior to the jugular tubercle lies the inner orifice of the hypoglossal canal. The petro-occipital sutures are oriented posteriorly and laterally and course from the foramen lacerum to the jugular foramen. The jugular tubercle is a bony prominence connecting the basal and lateral parts of the occipital bone. It is located 5 mm above and anterior to the hypoglossal canal and 8 mm medial to the medial edge of the jugular foramen (19-23). Its average length, width, and thickness (amount of medial bulging measured at the level of the hypoglossal canal) measure 16.5, 11.5, and 0.61 mm on average, respectively (22, 24). The hypoglossal canal is located in the jugular process of the lateral part of the occipital bone. It is oriented anteriorly, laterally, and superiorly, forming an angle with the sagittal plane ranging between 45° and 49° (21, 25-30). It opens laterally into the interval between the jugular foramen and carotid canal. The hypoglossal canal is also referred to as the anterior condylar canal and transmits the hypoglossal nerve (Figure 4A).

From the exocranial standpoint, the paramedian anterior skull base corridor is formed by the lateral plates of the ethmoid bone, which separate the nasal cavity from the orbits (Figure 2B). The paramedian middle skull base corridor is constituted by the pterygoid process of the sphenoid bone, which branches into medial and lateral pterygoid plates. Between the medial and lateral pterygoid plates, the pterygoid (scaphoid) fossa is beneath the floor of the paramedian middle skull base. In the sagittal plane, the length of the pterygoid process marks the anterior-posterior limits of the cavernous sinus (Figure 3F). The paramedian posterior skull base corridor involves the exocranial part of the petroclival fissure and the occipital condyle. When viewed from outside the cranium, the petroclival fissure appears as a deep cleft filled with a fibrocartilaginous tissue remnant of the primitive chondrocranium along which the inferior petroclival vein passes. The condyle is exocranial, generally oval, convex downward and outward, and articulates with the superior articular facet of the atlas, which conversely, is concave upward and inward. The condyles are located along the anterior half of the edge of the foramen magnum and extend forward and medially from three to one and nine to eleven o'clock (25, 31-33). The supracondylar fossa is a small depression lying posterior to the condyle that corresponds to the location of the jugular tubercle on the endocranial side (34). The posterior condylar vein runs within the posterior condylar canal of the supracondylar fossa (35, 36) (Figure 4B).

Lateral Skull Base Corridor

Regarding the transcranial approaches, the lateral anterior skull base corridor is composed of the orbital plates of the frontal bone anteriorly and the lesser sphenoid wings posteriorly; the medial portion of the lesser sphenoid wing forms the anterior clinoid processes (Figure 2A).

The lateral middle skull base corridor is composed of the lesser and greater sphenoid wings and the squamous and petrous parts of the temporal bone, forming the temporal fossae on both sides. The optic strut separates the optic canal from the superior orbital fissure and is the root of the lesser sphenoid wing on the lateral surface of the body of the sphenoid bone. The stout root of the greater sphenoid wing originates from the inferior part of the lateral sphenoid body and forms a large part of the temporal fossa floor. The superior orbital fissure lies between the lesser and greater sphenoid wings and is located lateral to the optic canal at the orbital apex. The superior orbital fissure transmits the first trigeminal division, the oculomotor, trochlear, and abducens nerves, and the inferior ophthalmic veins (Figure 3E). The lateral corridor involves the foramen rotundum, foramen ovale, foramen spinosum, and occasionally the foramen of Vesalius, when present. The foramen rotundum is separated from the superior orbital fissure by the maxillary strut and transmits the second trigeminal division. The foramen ovale transmits the third

trigeminal division, the motor trigeminal branch, the lesser superficial petrosal nerve, and in most cases, the accessory meningeal artery. The foramen spinosum is the most lateral of the three foramina and gives passage to the middle meningeal artery and spinosum nerve (branch of V3). The foramen spinosum is an important landmark for orientation during the middle fossa surgical approach. The foramen of Vesalius is medial to the foramen ovale when present; it transmits a vein connecting the pterygoid venous plexus and the cavernous sinus and may contain the accessory meningeal artery in some cases. On the petrous apex, the trigeminal impression forms the floor of Meckel's cave, which contains the Gasserian ganglion. Posterolaterally, the arcuate eminence overlies the superior semicircular canal. Lateral to the arcuate eminence, the tegmen tympani separates the middle fossa from the middle ear (Figure 3C-E). The lateral posterior skull base corridor involves the caudal half of the petro-occipital suture, the jugular foramen, the posterior aspect of the petrous bone including the internal auditory canal, and the sulcus of the sigmoid sinus.

At the inferior limit of the petro-occipital suture, the lateral part of the occipital bone, and the petrous part of the temporal bone form the jugular foramen. The notch on the jugular process of the occipital bone forms the posterior border of the jugular foramen; the anterior border is formed by the jugular fossa of the petrous part of the temporal bone (20, 37). The jugular foramen transmits the inferior petrosal sinus, sigmoid sinus, and glossopharyngeal, vagus, and accessory nerves.

The posterior surface of the petrous bone and the squamosal part of the occipital bone form the posterolateral skull base. On the posterior surface of the petrous bone, the internal auditory canal is located 5 mm above the jugular foramen and transmits the facial and vestibulocochlear nerves and the labyrinthine artery which arises from the anterior inferior cerebellar artery (19, 21).

The sulcus of the sigmoid sinus runs lateral to the medial from the astèrion to the jugular foramen. The astèrion is a craniometric point corresponding to the site where the lambdoid (parieto-occipital), parietomastoid, and occipitomastoid sutures meet. It generally overlies the point where the transverse sinus turns sharply inferiorly into the sigmoid sinus, but some variations are known (38-47) (Figure 4A).

On the exocranial surface, the orbital region is the site through which are directed several endoscopic approaches to the anterior and middle skull base (48-52) (Figure 2B). Laterally to the pterygoid fossa, the infratemporal fossa and the mandibular fossa form the remaining anterior and posterior part, respectively, of the lateral corridor of the middle skull base. The pterygopalatine fossa lies between the pterygoid process of the sphenoid bone posteriorly and the posterior wall of the maxillary sinus anteriorly (53). The medial boundary is the lateral pterygoid plate. Laterally, it opens into the infratemporal fossa through the pterygomaxillary fissure. The vidian canal, which transmits the vidian nerve and artery opens into the pterygopalatine fossa (54, 55).

The infratemporal fossa is bounded superiorly by the infratemporal crest of the sphenoid bone, anteriorly by the pterygomaxillary fissure, and posteriorly by the tympanic part of the temporal bone and the styloid process. Superiorly, the infratemporal fossa communicates with the temporal fossa; inferiorly, it blends into the parapharyngeal space (56, 57).

The mandibular fossa includes the mandibular condyle and is roofed by the tympanic and squamosal parts of the temporal bone. The squamotympanic fissure, along which the chorda tympani nerve passes, divides the mandibular fossa into an anterior and posterior part.

The parapharyngeal space is shaped like an inverted pyramid with the base formed by the greater wing of the sphenoid bone and the apex formed by the hyoid bone. The medial wall is formed by the superior pharyngeal constrictor muscle, the medial pterygoid muscle, ramus of the mandible, deep lobe of the parotid gland, and posterior belly of the digastric forms the lateral wall. Posteriorly, space is bounded by an extension of the prevertebral fascia. The parapharyngeal space is divided by the styloid diaphragm into prestyloid and retrostyloid compartments; the parapharyngeal internal carotid artery courses within the retrostyloid space (58-68). The foramen rotundum opens into the pterygopalatine fossa; the foramen ovale and foramen spinosum into the infratemporal fossa; and the jugular foramen into the parapharyngeal space (Figure 3F).

The exocranial posterolateral skull base is formed by the styloid, mastoid, and petrous parts of the temporal bone and the squamosal part of the occipital bone. The styloid process is the cranial point of attachment for the muscles of the styloid diaphragm. Posterior to the styloid process, the stylomastoid foramen transmits the facial nerve at its exit from the Fallopian canal. On the inferior exocranial surface of the petrous part of the temporal bone, the external orifice of the carotid canal is located anterior and medial to the jugular foramen. The jugular foramen and hypoglossal canal open into the parapharyngeal space. The mastoid part of the temporal bone forms the posterior border of the external acoustic meatus. The mastoid process is lateral to the styloid process, grooved by the occipital artery, and contains the mastoid emissary foramen for the mastoid emissary vein. The mastoid notch is the cranial point of attachment for the sternocleidomastoid and digastric muscles (Figure 4B).

Discussion

Thorough knowledge of the anatomy of the cranial base is the starting point for the execution of skull base approaches for the treatment of tumors and neurovascular pathologies as aneurysms, arteriovenous malformations, arteriovenous fistulas, and cavernous hemangiomas (69-73). The implementation of the modular concept has proved to be effective in the planning, execution, and tailoring of the skull base approaches (74-76). It is applicable to transcranial and endoscopic surgical routes and, in both cases, the mastery of the anatomical basis of the median, paramedian and lateral corridors is essential. The spatial topographic definition of each corridor should involve the sagittal, coronal, and axial plane, and any surgical target ought to be exactly localized at the level of one or more of these corridors. In the preoperative planning of surgery, computed tomography and magnetic resonance imaging should be complementary in allowing for precise localization of the lesion. Anterolateral transcranial approaches to the supratentorial region, including the pterional, supraorbital, orbitopterional, and cranio-orbitozygomatic, are executed through the lateral anterior and middle skull base corridors but allows to reach the midline neurovascular structures. The extensions of the frontotemporal approach, namely the drilling of the lesser sphenoid wing which characterizes the pterional approach, is aimed at exposing the sphenoidal compartment of the Sylvian fissure, thus widening the subfrontal perspectives until the midline (77). Orbitotomy and zygomatic osteotomy related to the orbitozygomatic approach, as well as anterior clinoidectomy, have the same objective. Similarly, intradural transcavernous posterior clinoidectomy, targeted at effectively expose basilar tip aneurysms, marks the transition between the paramedian and median corridor at the level of the upper clival region (78-80). The same transition occurs with the transcondylar extension of the far lateral approach, which is generally necessary to widening the working corridor to the ventral foramen magnum area (19, 23, 81). Further examples are the subtemporal transtentorial approach, Kawase approach, and presigmoid posterior petrosal or combined petrosal approach (82-85). In the extended endoscopic skull base approaches, the extension may involve the sagittal plane, coronal plane, or both. Some examples of the transition from the median to the paramedian corridor on the coronal plane are the transethmoidal approach to the optic canal and orbit, the transethmoidal transcribriform transfovea ethmoidalis approach to the anterior cranial fossa, the transmaxillary transpterygoid approach to the pterygopalatine fossa, infratemporal fossa, petrous apex, and the Meckel's cave, the "far-medial" transcondylar transjugular tubercle approach to the inferior third of the clivus, and the front door approach to the Meckel's cave (86-90). Recently, endoscopic approaches have been implemented also for those lesions mainly involving the paramedian corridor, as the orbital tumors or spheno-orbital meningiomas, or even the suprasellarar area (91-94).

In the last few years, neurosurgery has been characterized by tremendous advancements in all its fields, including the further improvement of endoscopic techniques, molecular biology of brain tumors, robotics, and virtual and augmented reality (95-107). Nevertheless, it must be stressed that perfect knowledge of the anatomy of the cranial base remains essential for the optimal planning and safe execution of any kind of approach.

Conclusion

Exhaustive knowledge of the three-dimensional anatomy of the cranial base and mastery of the modular concept are vital for the planning and execution of the transcranial and endoscopic approaches to skull base lesions.

Conflicts of interest: Each author declares that he or she has no commercial associations (e.g. consultancies, stock ownership, equity interest, patent/licensing arrangement etc.) that might pose a conflict of interest in connection with the submitted article.

References

1. Patel CR, Fernandez-Miranda JC, Wang WH, Wang EW. Skull Base Anatomy. Otolaryngol Clin North Am. 2016;49(1):9-20.
2. Standring S. Gray's Anatomy: The Anatomical Basis of Clinical Practice: Elsevier Limited; 2016.
3. Lang J. Skull Base and Related Structures: Atlas of Clinical Anatomy: Schattauer; 2001.
4. Rhoton AL, Jr. The anterior and middle cranial base. Neurosurgery. 2002;51(4 Suppl):S273-302.
5. Rhoton AL, Jr. The orbit. Neurosurgery. 2002;51(4 Suppl):S303-34.
6. Rhoton AL, Jr. The sellar region. Neurosurgery. 2002;51 (4 Suppl):S335-74.
7. Rhoton AL, Jr. The cavernous sinus, the cavernous venous plexus, and the carotid collar. Neurosurgery. 2002;51(4 Suppl):S375-410.
8. Salgado-López L, Campos-Leonel LCP, Pinheiro-Neto CD, Peris-Celda M. Orbital Anatomy: Anatomical Relationships of Surrounding Structures. J Neurol Surg B Skull Base. 2020;81(4):333-47.
9. Microsurgical Anatomy and Surgery of the Central Skull Base. American Journal of Neuroradiology. 2005;26(5):1292-3.
10. Stamm AC. Transnasal Endoscopic Skull Base and Brain Surgery: Surgical Anatomy and its Applications: Thieme; 2019.
11. Borba L, de Oliveira JG. Microsurgical and Endoscopic Approaches to the Skull Base: Anatomy, Tactics, and Techniques: Thieme Medical Publishers, Incorporated; 2021.
12. Hanna EY, DeMonte F. Comprehensive Management of Skull Base Tumors: Thieme; 2021.
13. Sanna M, Saleh EA. Atlas of Microsurgery of the Lateral Skull Base: Thieme; 2011.
14. Fisch U, Mattox DE. Microsurgery of the Skull Base: N.Y.; 1988.
15. Bassed RB, Briggs C, Drummer OH. Analysis of time of closure of the spheno-occipital synchondrosis using computed tomography. Forensic Sci Int. 2010;200(1-3):161-4.
16. Abdel Aziz KM, Sanan A, van Loveren HR, Tew JM, Jr., Keller JT, Pensak ML. Petroclival meningiomas: predictive parameters for transpetrosal approaches. Neurosurgery. 2000;47(1):139-50; discussion 50-2.
17. Luzzi S DMM, Elia A, Vincitorio F, Di Perna G, Zenga F, Garbossa D, Elbabaa S, Galzio R Morphometric and Radiomorphometric Study of the Correlation Between the Foramen Magnum Region and the Anterior and Posterolateral Approaches to Ventral Intradural Lesions. Turkish Neurosurgery. 2019;In Press.
18. Funaki T, Matsushima T, Peris-Celda M, Valentine RJ, Joo W, Rhoton AL, Jr. Focal transnasal approach to the upper, middle, and lower clivus. Neurosurgery. 2013;73(2 Suppl Operative):ons155-90; discussion ons90-1.
19. Wen HT, Rhoton AL, Jr., Katsuta T, de Oliveira E. Microsurgical anatomy of the transcondylar, supracondylar, and paracondylar extensions of the far-lateral approach. J Neurosurg. 1997;87(4):555-85.
20. Rhoton AL, Jr. The foramen magnum. Neurosurgery. 2000;47(3 Suppl):S155-93.
21. de Oliveira E, Rhoton AL, Jr., Peace D. Microsurgical anatomy of the region of the foramen magnum. Surg Neurol. 1985;24(3):293-352.
22. Mintelis A, Sameshima T, Bulsara KR, Gray L, Friedman AH, Fukushima T. Jugular tubercle: Morphometric analysis and surgical significance. J Neurosurg. 2006;105(5):753-7.
23. Ciappetta P, Occhiogrosso G, Luzzi S, D'Urso PI, Garribba AP. Jugular tubercle and vertebral artery/posterior inferior cerebellar artery anatomic relationship: a 3-dimensional angiography computed tomography anthropometric study. Neurosurgery. 2009;64(5 Suppl 2):429-36; discussion 36.
24. Luzzi S, Del Maestro M, Elia A, Vincitorio F, Di Perna G, Zenga F, et al. Morphometric and Radiomorphometric Study of the Correlation Between the Foramen Magnum Region and the Anterior and Posterolateral Approaches to Ventral Intradural Lesions. Turk Neurosurg. 2019.
25. Naderi S, Korman E, Citak G, Guvencer M, Arman C, Senoglu M, et al. Morphometric analysis of human occipital condyle. Clin Neurol Neurosurg. 2005;107(3):191-9.
26. Muthukumar N, Swaminathan R, Venkatesh G, Bhanumathy SP. A morphometric analysis of the foramen magnum region as it relates to the transcondylar approach. Acta Neurochir (Wien). 2005;147(8):889-95.
27. Karasu A, Cansever T, Batay F, Sabanci PA, Al-Mefty O. The microsurgical anatomy of the hypoglossal canal. Surgical and radiologic anatomy : SRA. 2009;31:363-7.
28. Katsuta T, Matsushima T, Wen HT, Rhoton AL. Trajectory of the hypoglossal nerve in the hypoglossal canal: significance for the transcondylar approach. Neurologia medico-chirurgica. 2000;40:206-9; discussion 10.
29. Kirdani MA. The normal hypoglossal canal. The American journal of roentgenology, radium therapy, and nuclear medicine. 1967;99(3):700--4.
30. Lang J, Hornung G. [The hypoglossal channel and its contents in the posterolateral access to the petroclival area]. Neurochirurgia. 1993;36:75-80.

31. Guidotti A. Morphometrical considerations on occipital condyles. Anthropologischer Anzeiger; Bericht über die biologisch-anthropologische Literatur. 1984;42(2):117--9.
32. Olivier G. Biometry of the human occipital bone. J Anat. 1975;120(Pt 3):507-18.
33. Bozbuga M, Ozturk A, Bayraktar B, Ari Z, Sahinoglu K, Polat G, et al. Surgical anatomy and morphometric analysis of the occipital condyles and foramen magnum. Okajimas Folia Anat Jpn. 1999;75(6):329-34.
34. Matsushima T, Kawashima M, Masuoka J, Mineta T, Inoue T. Transcondylar fossa (supracondylar transjugular tubercle) approach: anatomic basis for the approach, surgical procedures, and surgical experience. Skull Base. 2010;20(2):83-91.
35. Matsushima K, Kawashima M, Matsushima T, Hiraishi T, Noguchi T, Kuraoka A. Posterior condylar canals and posterior condylar emissary veins—a microsurgical and CT anatomical study. Neurosurgical Review. 2014;37(1):115-26.
36. Matsushima KaFTaKNaKHaKMaRAL. Microsurgical anatomy of the lateral condylar vein and its clinical significance. Neurosurgery. 2015;11 Suppl 2:135--45; discussion 45--6.
37. Williams PL. Gray's anatomy. Nervous System. 1995:1240-3.
38. Avci E, Kocaogullar Y, Fossett D, Caputy A. Lateral posterior fossa venous sinus relationships to surface landmarks. Surg Neurol. 2003;59(5):392-7; discussion 7.
39. Bozbuga M, Boran BO, Sahinoglu K. Surface anatomy of the posterolateral cranium regarding the localization of the initial burr-hole for a retrosigmoid approach. Neurosurg Rev. 2006;29(1):61-3.
40. da Silva EB, Jr., Leal AG, Milano JB, da Silva LF, Jr., Clemente RS, Ramina R. Image-guided surgical planning using anatomical landmarks in the retrosigmoid approach. Acta Neurochir (Wien). 2010;152(5):905-10.
41. Day JD, Kellogg JX, Tschabitscher M, Fukushima T. Surface and superficial surgical anatomy of the posterolateral cranial base: significance for surgical planning and approach. Neurosurgery. 1996;38:1079-83; discussion 83-4.
42. Day JD, Tschabitscher M. Anatomic position of the asterion. Neurosurgery. 1998;42(1):198-9.
43. Duangthongpon P, Thanapaisal C, Kitkhuandee A, Chaiciwamongkol K, Morthong V. The Relationships between Asterion, the Transverse-Sigmoid Junction, the Superior Nuchal Line and the Transverse Sinus in Thai Cadavers: Surgical Relevance. J Med Assoc Thai. 2016;99 Suppl 5:S127-S31.
44. Galindo-de León S, Hernández-Rodríguez AN, Morales-Ávalos R, Theriot-Girón MDC, Elizondo-Omaña RE, Guzmán-López S. Morphometric characteristics of the asterion and the posterolateral surface of the skull: its relationship with dural venous sinuses and its neurosurgical importance. Cir Cir. 2013;81(4):269-73.
45. Hall S, Peter Gan Y-C. Anatomical localization of the transverse-sigmoid sinus junction: Comparison of existing techniques. Surgical neurology international. 2019;10:186-.
46. Hwang RS, Turner RC, Radwan W, Singh R, Lucke-Wold B, Tarabishy A, et al. Relationship of the sinus anatomy to surface landmarks is a function of the sinus size difference between the right and left side: Anatomical study based on CT angiography. Surgical neurology international. 2017;8:58-.
47. Xia L, Zhang M, Qu Y, Ren M, Wang H, Zhang H, et al. Localization of transverse-sigmoid sinus junction using preoperative 3D computed tomography: application in retrosigmoid craniotomy. Neurosurgical review. 2012;35(4):593-9.
48. Dallan I, Di Somma A, Prats-Galino A, Solari D, Alobid I, Turri-Zanoni M, et al. Endoscopic transorbital route to the cavernous sinus through the meningo-orbital band: a descriptive anatomical study. Journal of Neurosurgery JNS. 2017;127(3):622-9.
49. Dallan I, Sellari-Franceschini S, Turri-Zanoni M, de Notaris M, Fiacchini G, Fiorini FR, et al. Endoscopic Transorbital Superior Eyelid Approach for the Management of Selected Spheno-orbital Meningiomas: Preliminary Experience. Operative Neurosurgery. 2017;14(3):243-51.
50. Di Somma A, Cavallo LM, de Notaris M, Solari D, Topczewski TE, Bernal-Sprekelsen M, et al. Endoscopic endonasal medial-to-lateral and transorbital lateral-to-medial optic nerve decompression: an anatomical study with surgical implications. Journal of Neurosurgery JNS. 2017;127(1):199-208.
51. Di Somma A, Andaluz N, Cavallo LM, de Notaris M, Dallan I, Solari D, et al. Endoscopic transorbital superior eyelid approach: anatomical study from a neurosurgical perspective. Journal of Neurosurgery JNS. 2018;129(5):1203-16.
52. Di Somma A, Andaluz N, Cavallo LM, Keller JT, Solari D, Zimmer LA, et al. Supraorbital vs Endo-Orbital Routes to the Lateral Skull Base: A Quantitative and Qualitative Anatomic Study. Operative Neurosurgery. 2018;15(5):567-76.
53. Chung HJ, Moon IS, Cho HJ, Kim CH, Sharhan SSA, Chang JH, et al. Analysis of Surgical Approaches to Skull Base Tumors Involving the Pterygopalatine and Infratemporal Fossa. J Craniofac Surg. 2019;30(2):589-95.
54. Labib MA, Prevedello DM, Carrau R, Kerr EE, Naudy C, Abou Al-Shaar H, et al. A road map to the internal carotid artery in expanded endoscopic endonasal approaches to the ventral cranial base. Neurosurgery. 2014;10 Suppl 3:448-71; discussion 71.
55. Barges-Coll J, Fernandez-Miranda JC, Prevedello DM, Gardner P, Morera V, Madhok R, et al. Avoiding injury to the abducens nerve during expanded endonasal endoscopic surgery: anatomic and clinical case studies. Neurosurgery. 2010;67(1):144-54; discussion 54.
56. Joo W, Funaki T, Yoshioka F, Rhoton AL, Jr. Microsurgical anatomy of the infratemporal fossa. Clin Anat. 2013;26(4):455-69.
57. Bejjani GKaSBaS-LEaAJaWDCaJAaSLN. Surgical anatomy of the infratemporal fossa: the styloid diaphragm revisited. Neurosurgery. 1998;43(4):842--52; discussion 52--3.

58. Bejjani GK, Sullivan B, Salas-Lopez E, Abello J, Wright DC, Jurjus A, et al. Surgical anatomy of the infratemporal fossa: the styloid diaphragm revisited. Neurosurgery. 1998;43(4):842-52; discussion 52-3.
59. Carrau RL, Myers EN, Johnson JT. Management of tumors arising in the parapharyngeal space. Laryngoscope. 1990;100(6):583-9.
60. Cohen SM, Burkey BB, Netterville JL. Surgical management of parapharyngeal space masses. Head Neck. 2005;27(8):669-75.
61. Dimitrijevic MV, Jesic SD, Mikic AA, Arsovic NA, Tomanovic NR. Parapharyngeal space tumors: 61 case reviews. Int J Oral Maxillofac Surg. 2010;39(10):983-9.
62. Eisele DE, Netterville JL, Hoffman HT, Gantz BJ. Parapharyngeal space masses. Head Neck. 1999;21(2):154-9.
63. Khafif A, Segev Y, Kaplan DM, Gil Z, Fliss DM. Surgical management of parapharyngeal space tumors: a 10-year review. Otolaryngol Head Neck Surg. 2005;132(3): 401-6.
64. Luzzi S, Giotta Lucifero A, Del Maestro M, Marfia G, Navone SE, Baldoncini M, et al. Anterolateral Approach for Retrostyloid Superior Parapharyngeal Space Schwannomas Involving the Jugular Foramen Area: A 20-Year Experience. World Neurosurg. 2019.
65. Shahinian H, Dornier C, Fisch U. Parapharyngeal space tumors: the infratemporal fossa approach. Skull Base Surg. 1995;5(2):73-81.
66. Som PM, Biller HF, Lawson W. Tumors of the parapharyngeal space: preoperative evaluation, diagnosis and surgical approaches. Ann Otol Rhinol Laryngol Suppl. 1981;90(1 Pt 4):3-15.
67. Stell PM, Mansfield AO, Stoney PJ. Surgical approaches to tumors of the parapharyngeal space. Am J Otolaryngol. 1985;6(2):92-7.
68. Ferrari M, Schreiber A, Mattavelli D, Lombardi D, Rampinelli V, Doglietto F, et al. Surgical anatomy of the parapharyngeal space: Multiperspective, quantification-based study. Head & Neck. 2019;41(3):642-56.
69. Luzzi S, Del Maestro M, Elbabaa SK, Galzio R. Letter to the Editor Regarding "One and Done: Multimodal Treatment of Pediatric Cerebral Arteriovenous Malformations in a Single Anesthesia Event". World Neurosurg. 2020;134:660.
70. Luzzi S, Gragnaniello C, Giotta Lucifero A, Del Maestro M, Galzio R. Surgical Management of Giant Intracranial Aneurysms: Overall Results of a Large Series. World Neurosurg. 2020;144:e119-e37.
71. Luzzi S, Gragnaniello C, Giotta Lucifero A, Del Maestro M, Galzio R. Microneurosurgical management of giant intracranial aneurysms: Datasets of a twenty-year experience. Data Brief. 2020;33:106537.
72. Del Maestro M, Rampini AD, Mauramati S, Giotta Lucifero A, Bertino G, Occhini A, et al. Dye-Perfused Human Placenta for Vascular Microneurosurgery Training: Preparation Protocol and Validation Testing. World Neurosurg. 2020.
73. Luzzi S, Del Maestro M, Galzio R. Letter to the Editor. Preoperative embolization of brain arteriovenous malformations. J Neurosurg. 2019;132(6):2014-6.
74. Kassam AB, Prevedello DM, Carrau RL, Snyderman CH, Thomas A, Gardner P, et al. Endoscopic endonasal skull base surgery: analysis of complications in the authors' initial 800 patients. J Neurosurg. 2011;114(6):1544-68.
75. Kassam A, Snyderman CH, Mintz A, Gardner P, Carrau RL. Expanded endonasal approach: the rostrocaudal axis. Part I. Crista galli to the sella turcica. Neurosurgical Focus FOC. 2005;19(1):1-12.
76. Kassam A, Snyderman CH, Mintz A, Gardner P, Carrau RL. Expanded endonasal approach: the rostrocaudal axis. Part II. Posterior clinoids to the foramen magnum. Neurosurgical Focus FOC. 2005;19(1):1-7.
77. Yaşargil MG. Microneurosurgery: Thieme; 1984.
78. Krisht AF. Transcavernous approach to diseases of the anterior upper third of the posterior fossa. Neurosurg Focus. 2005;19(2):E2.
79. Krisht AF, Kadri PA. Surgical clipping of complex basilar apex aneurysms: a strategy for successful outcome using the pretemporal transzygomatic transcavernous approach. Neurosurgery. 2005;56(2 Suppl):261-73; discussion -73.
80. Krisht AF, Krayenbuhl N, Sercl D, Bikmaz K, Kadri PA. Results of microsurgical clipping of 50 high complexity basilar apex aneurysms. Neurosurgery. 2007;60(2):242-50; discussion 50-2.
81. Heros RC. Lateral suboccipital approach for vertebral and vertebrobasilar artery lesions. J Neurosurg. 1986;64(4): 559-62.
82. Kawase T, Toya S, Shiobara R, Mine T. Transpetrosal approach for aneurysms of the lower basilar artery. J Neurosurg. 1985;63(6):857-61.
83. Al-Mefty O, Fox JL, Smith RR. Petrosal approach for petroclival meningiomas. Neurosurgery. 1988;22(3):510-7.
84. Drake CG. Bleeding aneurysms of the basilar artery. Direct surgical management in four cases. J Neurosurg. 1961;18:230-8.
85. Drake CG. Bleeding aneurysms of the basilar artery. Direct surgical management in four cases. 1961. Can J Neurol Sci. 1999;26(4):335-40.
86. Akdemir G, Tekdemir I, Altin L. Transethmoidal approach to the optic canal: surgical and radiological microanatomy. Surg Neurol. 2004;62(3):268-74; discussion 74.
87. Greenfield JP, Anand VK, Kacker A, Seibert MJ, Singh A, Brown SM, et al. Endoscopic endonasal transethmoidal transcribriform transfovea ethmoidalis approach to the anterior cranial fossa and skull base. Neurosurgery. 2010;66(5):883-92; discussion 92.
88. Hofstetter CP, Singh A, Anand VK, Kacker A, Schwartz TH. The endoscopic, endonasal, transmaxillary transpterygoid approach to the pterygopalatine fossa, infratemporal fossa, petrous apex, and the Meckel cave. J Neurosurg. 2010;113(5):967-74.
89. Morera VA, Fernandez-Miranda JC, Prevedello DM, Madhok R, Barges-Coll J, Gardner P, et al. "Far-medial"

expanded endonasal approach to the inferior third of the clivus: the transcondylar and transjugular tubercle approaches. Neurosurgery. 2010;66(6 Suppl Operative):211-9; discussion 9-20.
90. Kassam AB, Prevedello DM, Carrau RL, Snyderman CH, Gardner P, Osawa S, et al. The front door to meckel's cave: an anteromedial corridor via expanded endoscopic endonasal approach- technical considerations and clinical series. Neurosurgery. 2009;64(3 Suppl):ons71-82; discussion ons-3.
91. Luzzi S, Zoia C, Rampini AD, Elia A, Del Maestro M, Carnevale S, et al. Lateral Transorbital Neuroendoscopic Approach for Intraconal Meningioma of the Orbital Apex: Technical Nuances and Literature Review. World Neurosurg. 2019;131:10-7.
92. Peron S, Cividini A, Santi L, Galante N, Castelnuovo P, Locatelli D. Spheno-Orbital Meningiomas: When the Endoscopic Approach Is Better. Acta Neurochir Suppl. 2017;124:123-8.
93. Zoia C, Bongetta D, Dorelli G, Luzzi S, Maestro MD, Galzio RJ. Transnasal endoscopic removal of a retrochiasmatic cavernoma: A case report and review of literature. Surg Neurol Int. 2019;10:76.
94. Arnaout MM, Luzzi S, Galzio R, Aziz K. Supraorbital keyhole approach: Pure endoscopic and endoscope-assisted perspective. Clin Neurol Neurosurg. 2019;189:105623.
95. Gardner PA, Vaz-Guimaraes F, Jankowitz B, Koutourousiou M, Fernandez-Miranda JC, Wang EW, et al. Endoscopic Endonasal Clipping of Intracranial Aneurysms: Surgical Technique and Results. World Neurosurg. 2015;84(5):1380-93.
96. Heiferman DM, Somasundaram A, Alvarado AJ, Zanation AM, Pittman AL, Germanwala AV. The endonasal approach for treatment of cerebral aneurysms: A critical review of the literature. Clin Neurol Neurosurg. 2015;134:91-7.
97. Palumbo P, Lombardi F, Augello FR, Giusti I, Luzzi S, Dolo V, et al. NOS2 inhibitor 1400W Induces Autophagic Flux and Influences Extracellular Vesicle Profile in Human Glioblastoma U87MG Cell Line. Int J Mol Sci. 2019;20(12).
98. Luzzi S, Crovace AM, Del Maestro M, Giotta Lucifero A, Elbabaa SK, Cinque B, et al. The cell-based approach in neurosurgery: ongoing trends and future perspectives. Heliyon. 2019;5(11).
99. Raysi Dehcordi S, Ricci A, Di Vitantonio H, De Paulis D, Luzzi S, Palumbo P, et al. Stemness Marker Detection in the Periphery of Glioblastoma and Ability of Glioblastoma to Generate Glioma Stem Cells: Clinical Correlations. World Neurosurg. 2017;105:895-905.
100. Giotta Lucifero A, Luzzi S, Brambilla I, Trabatti C, Mosconi M, Savasta S, et al. Innovative therapies for malignant brain tumors: the road to a tailored cure. Acta Biomed. 2020;91(7-s):5-17.
101. Dorfer C, Rydenhag B, Baltuch G, Buch V, Blount J, Bollo R, et al. How technology is driving the landscape of epilepsy surgery. Epilepsia. 2020;61(5):841-55.
102. Cho J, Rahimpour S, Cutler A, Goodwin CR, Lad SP, Codd P. Enhancing Reality: A Systematic Review of Augmented Reality in Neuronavigation and Education. World Neurosurg. 2020;139:186-95.
103. Bellantoni G, Guerrini F, Del Maestro M, Galzio R, Luzzi S. Simple schwannomatosis or an incomplete Coffin-Siris? Report of a particular case. eNeurologicalSci. 2019;14:31-3.
104. McBeth PB, Louw DF, Rizun PR, Sutherland GR. Robotics in neurosurgery. The American Journal of Surgery. 2004;188(4):68-75.
105. Rohde V, Spangenberg P, Mayfrank L, Reinges M, Gilsbach JM, Coenen VA. Advanced neuronavigation in skull base tumors and vascular lesions. Minim Invasive Neurosurg. 2005;48(1):13-8.
106. Snyderman CH, Carrau RL, Prevedello DM, Gardner P, Kassam AB. Technologic innovations in neuroendoscopic surgery. Otolaryngol Clin North Am. 2009;42(5):883-90, x.
107. Luzzi S, Giotta Lucifero A, Martinelli A, Maestro MD, Savioli G, Simoncelli A, et al. Supratentorial high-grade gliomas: maximal safe anatomical resection guided by augmented reality high-definition fiber tractography and fluorescein. Neurosurg Focus. 2021;51(2):E5.

Correspondence:
Received: 5 July 2021
Accepted: 5 August 2021
Sabino Luzzi MD, PhD, Neurosurgery Unit,
Department of Clinical-Surgical,
Diagnostic and Pediatric Sciences, University of Pavia,
Pavia, Italy;
Neurosurgery Unit,
Department of Surgical Sciences,
Fondazione IRCCS Policlinico San Matteo, Pavia, Italy,
Phone: +39 0382502781, +39 0382502780;
E-mail: sabino.luzzi@unipv.it